HHS Public Access

Author manuscript

Cell Rep. Author manuscript; available in PMC 2019 March 20.

Published in final edited form as:

Cell Rep. 2019 March 12; 26(11): 3076–3086.e6. doi:10.1016/j.celrep.2019.02.054.

FOXM1 Deubiquitination by USP21 Regulates Cell Cycle Progression and Paclitaxel Sensitivity in Basal-like Breast Cancer

Anthony Arceci[1,2], **Thomas Bonacci**[2], **Xianxi Wang**[2], **Kyle Stewart**[2], **Jeffrey S. Damrauer**[2,3], **Katherine A. Hoadley**[2,3], and **Michael J. Emanuele**[1,2,4,5,*]

[1]Curriculum in Genetics and Molecular Biology, The University of North Carolina at Chapel Hill, Chapel Hill, NC 27599, USA

[2]Lineberger Comprehensive Cancer Center, The University of North Carolina at Chapel Hill, Chapel Hill, NC 27599, USA

[3]Department of Genetics, The University of North Carolina at Chapel Hill, Chapel Hill, NC 27599, USA

[4]Department of Pharmacology, The University of North Carolina at Chapel Hill, Chapel Hill, NC 27599, USA

[5]Lead Contact

SUMMARY

The transcription factor FOXM1 contributes to cell cycle progression and is significantly upregulated in basal-like breast cancer (BLBC). Despite its importance in normal and cancer cell cycles, we lack a complete understanding of mechanisms that regulate FOXM1. We identified USP21 in an RNAi-based screen for deubiquitinases that control FOXM1 abundance. USP21 increases the stability of FOXM1, and USP21 binds and deubiquitinates FOXM1 *in vivo* and *in vitro*, indicating a direct enzyme-substrate relationship. Depleting USP21 downregulates the FOXM1 transcriptional network and causes a signifi-cant delay in cell cycle progression. Significantly, USP21 depletion sensitized BLBC cell lines and mouse xenograft tumors to paclitaxel, an anti-mitotic, frontline therapy in BLBC treatment. USP21 is the most frequently amplified deubiquitinase in BLBC patient tumors, and its amplification co-occurs with the upregulation of FOXM1 protein. Altogether, these data suggest a role for USP21 in the proliferation and potentially treatment of FOXM1-high, USP21-high BLBC.

*Correspondence: emanuele@email.unc.edu.

AUTHOR CONTRIBUTIONS

A.A. designed, performed, and analyzed most cell biological experiments described and wrote and revised the manuscript. T.B. performed the *in vivo* deubiquitination experiment and provided critical revisions to the manuscript. X.W. performed the FOXM1 transcriptional reporter assay. K.S. maintained mice and collected data associated with the described tumor xenograft experiment. J.S.D. and K.A.H. performed the bioinformatic analysis of TCGA data-sets. M.J.E. designed experiments, helped analyze data, and provided critical revisions to the manuscript.

SUPPLEMENTAL INFORMATION

Supplemental Information can be found with this article online at https://doi.org/10.1016/j.celrep.2019.02.054.

DECLARATION OF INTERESTS

The authors declare no competing interests.

Graphical Abstract

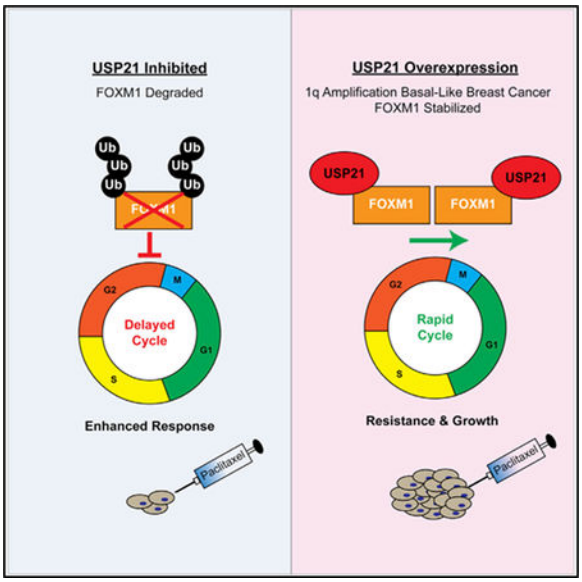

In Brief

The cell cycle transcription factor FOXM1 is activated in basal-like breast cancer (BLBC) and associated with therapeutic resistance and poor patient outcomes. Arceci et al. show USP21 antagonizes FOXM1 degradation, thereby promoting proliferation and paclitaxel resistance. USP21 is catalytically active and recurrently overexpressed in BLBC, representing a potential therapeutic target.

INTRODUCTION

FOXM1 is a member of the forkhead box family of transcription factors, composed of 44 members in humans, all of which share a conserved forkhead DNA-binding motif (Golson and Kaestner, 2016; Hannenhalli and Kaestner, 2009). FOX family transcription factors are involved in numerous processes and play particularly important roles in stem cell differentiation, proliferation, cell cycle, and metabolism (Myatt and Lam, 2007). FOXM1 is best known for its role in regulating the cell cycle, primarily through the transcription of a set of targets involved in establishing timely entry into and progression through mitosis (Chen et al., 2013; Grant et al., 2013; Laoukili et al., 2005; Sadasivam et al., 2012) and ensuring chromosome stability (Laoukili et al., 2005). In addition to its important role in normal cell cycles, the periodically expressed cell cycle genes controlled by FOXM1 are significantly upregulated in specific cancers and cancer subtypes (Cancer Genome Atlas Network, 2012; Cancer Genome Atlas Research Network, 2011; Hoadley et al., 2014).

Breast cancers are stratified into five subtypes, based on molecular features and transcriptome-based analysis, that predict outcomes and guide treatment paradigms. The molecularly defined basal-like breast cancer (BLBC) subtype largely overlaps with the triple-negative classification, named for a lack of overexpression of estrogen receptor (ER), progesterone receptor (PR), and *HER2* genes (Perou et al., 2000; Sorlie et al., 2003).

Outside of mutations to *TP53*, occurring in 80% of patient tumors, BLBC lacks recurrent somatic mutations to known oncogenes and instead exhibits a high degree of chromosome instability in the form of copy-number gains and losses, as well as severe aneuploidy (Cancer Genome Atlas Network, 2012; Hoadley et al., 2014). Upregulation of the FOXM1 transcriptional signature represents a defining feature of the BLBC subtype and related malignancies, such as high-grade serous ovarian cancer (Cancer Genome Atlas Network, 2012). Despite the upregulation of FOXM1 in BLBC, it is largely unknown how FOXM1 is activated in patient tumors. Because of its roles in the promotion of both cancer and chemotherapy resistance (Carr et al., 2010; Zhao et al., 2014), FOXM1 represents an attractive anti-cancer treatment target (Halasi and Gartel, 2013a).

FOXM1 is cell cycle regulated, with peak expression and activity occurring during the G2/M phase (Korver et al., 1997). FOXM1 is controlled by various post-translational modifications, including phosphorylation (Fu et al., 2008; Laoukili et al., 2008b; Major et al., 2004) and small ubiquitin-like modifier (SUMO)ylation (Myatt et al., 2014; Schimmel et al., 2014); however, it is unclear how these might account for its upregulation in cancer. Ubiquitination also plays an important role in FOXM1 regulation. FOXM1 and many of its transcriptional targets are ubiquitinated by the anaphase-promoting complex/cyclosome (APC/C), thereby triggering their degradation following the onset of mitosis (Laoukili et al., 2008a; Park et al., 2008). Ubiquitination of FOXM1 by Cul4-VprBP (Wang et al., 2017), RNF168 (Kong-sema et al., 2016), SCF-FBXO31 (Jeffery et al., 2017), and FBXW7 (Chen et al., 2016) has also been reported. This points to a pivotal role for ubiquitination-dependent degradation in regulating FOXM1.

A potential strategy for inactivating FOXM1 may exist by targeting enzymes that prevent FOXM1 destruction. To that end, we sought to identify deubiquitinating enzymes (DUBs) that regulate FOXM1 stability through the removal of ubiquitin, thus protecting FOXM1 from degradation. DUBs are catalytic proteases that remove ubiquitin from substrates with high *in vivo* selectivity. The human genome encodes approximately 100 DUBs, which are grouped into a growing number of subfamilies (Komander et al., 2009). Several selective small-molecule DUB inhibitors have been developed, pointing to their potential drugg-ability (Kategaya et al., 2017; Turnbull et al., 2017).

By deploying an RNAi-based screen against nucleus-localized DUBs, ubiquitin-specific protease 21 (USP21) was identified as a potential regulator of FOXM1 stability. USP21 is a member of the ubiquitin-specific protease (USP) family of DUBs, which contains 56 members unified by a highly conserved USP domain, featuring a catalytic triad essential for activity (Komander et al., 2009). USP21 has been linked to transcriptional regulation through interaction with the transcription factors NANOG (Jin et al., 2016), GATA3 (Zhang et al., 2013), and GLI1 (Heride et al., 2016) as well as histone H2A (Nakagawa et al., 2008).

Here, we demonstrate a substrate-enzyme relationship between FOXM1 and USP21. USP21 regulates FOXM1 abundance and USP21 binds and removes polyubiquitin chains from FOXM1, thus protecting it from proteasomal degradation. We also show that USP21 expression can alter the FOXM1 transcriptional network, which has consequences in regulating mitotic timing and proliferation. Furthermore, we show that FOXM1 and USP21

are specifically upregulated in BLBC and that depletion of USP21 can improve sensitivity to paclitaxel, primarily through its relationship with FOXM1. These findings demonstrate that USP21, through the maintenance of FOXM1 stability, regulates cell cycle progression and that inhibiting USP21 has therapeutic potential in treating BLBC with a FOXM1-high, USP21-high expression signature.

RESULTS

USP21 Binds and Alters FOXM1 Abundance

To determine whether FOXM1 abundance is regulated by DUB activity, HeLa cells were treated with PR-619, a small-molecule, non-specific pan-DUB inhibitor for 8 h. Immunoblot (IB) analysis revealed that FOXM1 abundance significantly decreased with increasing concentrations of PR-619 (Figure 1A). This suggested that the degradation of FOXM1 could be actively prevented by DUBs.

To discover specific USP-family DUBs that directly affect FOXM1 abundance, HeLa cells were transfected with pooled small interfering RNAs (siRNAs) against a subset of USP-family DUBs that show nuclear localization. IB analysis of cell lysates 48 h after transfection revealed that USP21 knockdown reproducibly reduced the level of endogenous FOXM1 (Figure 1B). Deconvolution of the siRNA pool revealed that multiple, independent siRNAs reagents targeting USP21 reduced the protein levels of FOXM1 (Figure S1A). Furthermore, FOXM1 abundance was not significantly reduced in cells stably expressing a FLAG- and hemagglutinin (HA)-tagged USP21 variant made resistant to USP21 siRNA (Figure S1B), demonstrating that the reduction in FOXM1 abundance is specifically linked to an on-target effect of USP21 knockdown. Correspondingly, ectopic expression of USP21 significantly increased FOXM1 abundance in 293T cells (Figure 1C). These results demonstrate that FOXM1 abundance is regulated by USP21.

To determine whether the effects on FOXM1 stability resulting from changes of USP21 expression were due to an interaction between the two proteins, FLAG- or HA-tagged FOXM1b and Myc-USP21 plasmids were ectopically expressed in 293T cells. An interaction between FOXM1 and USP21 was detected by coimmunoprecipitation (co-IP), regardless of whether the immuno-precipitation (IP) was directed against Myc-USP21 (Figure 1D) or HA-FOXM1b (Figure 1E). In addition, an interaction between endogenous FOXM1 and USP21 was detected using antibodies directed against USP21 (Figure 1F). To determine the domain on FOXM1 recognized by USP21, a series of Myc-FOXM1b fragments (Figure S1C) was co-transfected with FLAG-HA-USP21 into 293T cells and interactions were assessed by co-IP. Results from IP directed against both Myc-FOXM1b (Figure S1D) and FLAG-HA-USP21 (Figure S1E) demonstrate that USP21 binds to a region encompassing FOXM1 amino acids 321–400.

Because exogenous and endogenous FOXM1 and USP21 can interact *in vivo*, we assessed their binding *in vitro* by incubating recombinant, bacterially produced hexa-histidine (6xHIS)-tagged FOXM1b with recombinant, bacterially produced, glutathione S-transferase (GST)-tagged USP21. 6xHIS-FOXM1b was detected in complex with GST-USP21 following pull-down on glutathione resin (Figure 1G). Altogether, these data demonstrate

that USP21 and FOXM1 directly interact, strongly suggesting an enzyme-substrate relationship between the two proteins.

FOXM1 Is a USP21 Substrate

FOXM1 is a known substrate of several E3-ubiquitin ligases, including APC/C (Laoukili et al., 2008a; Park et al., 2008) and Cul4-VprBP (Wang et al., 2017), which can conjugate polyubiquitin chains onto FOXM1, triggering its subsequent proteasomal degradation. To determine whether the effects that USP21 knockdown or overexpression has on FOXM1 are mediated through proteasomal degradation, HeLa cells transfected with siRNA targeting firefly luciferase (siFF; control) or siRNA targeting USP21 (siUSP21) were treated with the proteasome inhibitor MG132. IB analysis confirms that FOXM1 destabilization resulting from USP21 knockdown is partially rescued through protea-some inhibition (Figure 2A).

DUBs oppose proteasomal degradation through removal of polyubiquitin chains, particularly K48 and K11 topologies, and USP21 has been shown to cleave both of these polyubiquitin linkages *in vitro* (Ye et al., 2011). To determine whether USP21 influences polyubiquitin chain conjugation on FOXM1, we analyzed FOXM1 ubiquitination *in vivo*. 293T cells were transfected with HA-FOXM1b and 6xHIS-FLAG-Ubiquitin in combination with either wild-type USP21 ($USP21^{WT}$) or a catalytically dead variant of USP21 (cystine at amino acid position 221 changed to alanine; $USP21^{C221A}$). 24 h post-transfection, cells were harvested and lysed under denaturing conditions, subjected to pull-down on nickel-charged nitrilotriacetic acid (Ni-NTA) resin to enrich for ubiquitinated proteins, and analyzed by IB. Polyubiquitinated FOXM1 (FOXM1 ≥ 100 kDa at the top of Figure 2B) was readily detectable under conditions with endogenous levels of USP21 expression (Figure 2B, lane 2), but it was greatly diminished by overexpression of $USP21^{WT}$ (Figure 2B, lane 3). However, levels of polyubiquitinated FOXM1 were restored close to levels observed in control conditions when $USP21^{C221A}$ was overexpressed (Figure 2B, lane 4). Similarly, $USP21^{WT}$, but not $USP21^{C221A}$, immunopurified from 293T cells reduced polyubiquitination of FOXM1 isolated from proteasome inhibitor-treated 293T cells in an *in vitro* deubiquitination assay (Figure S2A).

Because USP21 can directly bind and deubiquitinate FOXM1, we next evaluated the impact of USP21 on FOXM1 stability. To assess the effect of USP21 on FOXM1 half-life, FOXM1 levels were assessed by IB following overexpression of either $USP21^{WT}$ or $USP21^{C221A}$ in 293T cells (Figure 2C) and depletion of USP21 in BLBC MDA-MB-231 cells (Figure S2B) treated with cycloheximide to block protein translation. FOXM1 abundance decreases with similar kinetics over the first 4 h following cycloheximide treatment in all conditions, but $USP21^{WT}$ overexpression can protect the remaining population from degradation for at least another 12 h, whereas FOXM1 abundance falls even more rapidly in $USP21^{C221A}$ cells than in control cells after this point (Figure 2C). Half-life quantified from the best-fit curve for FOXM1 in control cells is approximately 7.6 h. The expression of $USP21^{WT}$ increased FOXM1 stability, and its half-life was approximately 12.4 h. In contrast, ectopic expression of $USP21^{C221A}$ shortened FOXM1 half-life to approximately 3.7 h, consistent with it having a dominant-negative effect on FOXM1 stability, as well as controlling its own ubiquitination (Figure S2B). Similarly, depletion of USP21 in MDA-MB-231 reduced FOXM1 half-life

from 11.5 to 4.2 h (Figure S2C). Altogether, these results indicate that USP21 controls FOXM1 ubiquitination and proteasomal-mediated degradation.

USP21 Affects the FOXM1 Transcriptional Network and Proliferation

FOXM1 is the master transcriptional regulator of a set of genes involved in establishing and ensuring a successful G2/M transition and progression through mitosis. Dysregulation of this transcriptional network has been shown to induce cell cycle delays, mitotic defects, and mis-segregation of chromosomes (Laoukili et al., 2005). We hypothesized that modulating USP21 levels would have corresponding effects on FOXM1 transcriptional output because of its effects on stabilizing FOXM1. To determine the effect that USP21 overexpression has on FOXM1 activity, 293T cells were co-transfected with USP21 and a FOXM1 luciferase-based transcriptional activity reporter (6x-DBE) (Furuyama et al., 2000). USP21 overexpression significantly enhanced FOXM1-dependent transcriptional activity compared with control (Figure 3A). This is consistent with our previous data demonstrating that FOXM1 abundance is positively enhanced by USP21 overexpression. Correspondingly, a panel of FOXM1 transcriptional targets was assessed by RT-qPCR following siRNA transfection to knockdown either FOXM1 or USP21 in MDA-MB-231 cells. Knockdown of USP21 leads to a reduction in all FOXM1 transcriptional targets assessed compared with controls (Figure 3B, compare red bars to black bars). USP21 knockdown did not lead to the same decrease in FOXM1 transcriptional target abundance as FOXM1 knockdown (Figure 3B, compare red bars to orange bars); however, this is consistent with biochemical data demonstrating that USP21 knockdown reduces FOXM1 levels to an amount between what is observed in control conditions and what is observed in FOXM1 knockdown conditions (Figure 3C). In addition, USP21 over-expression did not significantly alter *FOXM1* mRNA levels in MDA-MB-231 cells transduced with a pINDUCER20 lentivirus to introduce a doxycycline-inducible USP21 transgene (Meerbrey et al., 2011) (Figure S3A). Altogether, these data demonstrate that changes in FOXM1 levels because of USP21 have downstream effects on the FOXM1 transcriptional network.

Tight regulation of the FOXM1 transcriptional network is required for a timely and high-fidelity transition from G2 to mitosis. Having demonstrated that USP21 levels can affect the FOXM1 transcriptional network, we next sought to determine whether the kinetics of mitotic entry are disrupted by USP21 loss. To observe effects on mitotic timing, the accumulation of phospho-histone H3 S10 (P-H3) following release of cells from synchronization at the G1/S boundary with aphidicolin was monitored in MDA-MB-231 cells depleted of FOXM1 or USP21. In parallel, we analyzed cells in which FOXM1 was ectopically expressed in USP21-depleted cells (Figure S3B). Following release from synchronization, cells were treated with the microtubule poison nocodazole so that they would get trapped in mitosis, allowing us to determine the percentage of cells that had entered mitosis throughout the duration of the experiment. Depletion of either FOXM1 or USP21 significantly impaired cell cycle progression into mitosis. 22 h after release, only 1.6% and 10.9% of cells were P-H3 positive in FOXM1- and USP21-depleted populations, respectively (Figure 3D; Figure S4). In contrast, 40.7% of control cells had entered mitosis by that time. Mitotic entry was significantly rescued (27.4% of cells were P-H3 positive) in the USP21-depleted-FOXM1 overexpression populations. These results confirm prior reports that FOXM1 knockdown

impairs mitotic entry (Laoukili et al., 2005). Furthermore, they demonstrate that USP21 promotes progression through mitosis, because its depletion severely impairs the accumulation of mitotic cells. Because this defect is largely rescued by forced FOXM1 expression, the cell cycle phenotype in USP21-depleted cells occurs largely because of the reduction of FOXM1 abundance.

Finally, we hypothesized that slowed mitotic entry resulting from FOXM1 and USP21 knockdown would cause a corresponding reduction in proliferation. Proliferation was significantly impaired in the BLBC cell lines MDA-MB-468 and MDA-MB-231 (Figure 3E). In addition, ectopic, doxycyclineinducible expression of FOXM1b in MDA-MB-231 cells partially rescued the impaired proliferation caused by USP21 depletion. Similar results were observed in HeLa cells over a four-day period (Figure S3C). Thus, downregulation of USP21 can affect overall proliferation by downregulating both FOXM1 stability and downstream effects of the FOXM1 transcriptional network.

USP21 Amplification Correlates with FOXM1 Protein Levels and Tumor Proliferation in BLBC

FOXM1 upregulation has been reported in various cancers (Cancer Genome Atlas Network, 2012; Cancer Genome Atlas Research Network, 2011; Kalin et al., 2006; Kim et al., 2006; Liu et al., 2006). In breast cancer, we found that *FOXM1* mRNA expression is significantly correlated with breast cancer sub-types, showing the highest expression in the BLBC subtype (t test basal versus non-basal, $p \leq 2.2 \times 10^{-16}$) (Figure 4A, top). This is consistent with prior genomic studies that found the FOXM1 transcriptional signature upregulated in BLBC (Cancer Genome Atlas Network, 2012). We next analyzed the proliferative capacity of tumors in which FOXM1 is activated. The proliferation score of individual tumors was highly and significantly correlated with *FOXM1* expression, both across all breast cancer subtypes and within individual subtypes. That is, a tumor proliferation score increases as a function of *FOXM1* mRNA expression among all patient breast tumors even within only the luminal A breast cancers (Figure 4A, top, blue dots), which generally proliferate more slowly than more aggressive HER2-enriched and BLBC subtypes. As expected, expression analysis of well-established FOXM1 transcriptional targets revealed a corresponding upregulation in FOXM1-high, BLBC patient samples (Figure 4A, bottom). We conclude that *FOXM1* expression and activity exist on a sliding scale, with increasing *FOXM1* levels alone being a strong indicator of tumor proliferation.

Next, we analyzed copy number changes and mRNA expression for all human DUBs among breast tumors in the The Cancer Genome Atlas (TCGA) dataset. *USP21* is the fourth-most frequently copy number alteration (CNA)-amplified and the most frequently mRNA-overexpressed DUB across all patient samples (Figure 4B), with *USP21* amplification significantly correlated with both proliferation score and BLBC subtype (Figure S5A). The genomic location of *USP21* is 1q23. This region is the most frequently amplified region in BLBC patient tumors (Silva et al., 2015; Weigman et al., 2012). However, this amplicon lacks a well-described oncogene that contributes to disease. Correspondingly, IB analysis of FOXM1 and USP21 protein expression in cell lines representing the normal-like, luminal,

and BLBC subtypes of breast cancer revealed that expression of FOXM1 and USP21 is uniquely high in the BLBC subtypes (Figure 4C; Figure S5B).

FOXM1 is among the 227 proteins and/or antigens profiled by reverse-phase protein array (RPPA) in TCGA. This provided us the opportunity to examine the abundance of FOXM1 protein levels in breast cancer and its relationship to *USP21* mRNA expression in tumors. Because our results demonstrate that the FOXM1 protein is post-translationally stabilized by USP21, we examined FOXM1 protein levels as a function of *USP21* expression. FOXM1 protein is the most significantly upregulated protein and/or antigen in *USP21*-amplified tumors (Figure 4D). Among the other most statistically significant increasing proteins were the FOXM1 targets cyclin B1, the cell cycle-regulated gene MSH6 (Fischer et al., 2016), adenosine deaminase ADAR1 (which is proximal to the genetic location of USP21), and the asparagine deaminase ASNS, which has been previously implicated in breast cancer proliferation and cell cycle progression (Yang et al., 2014). Because FOXM1 is upregulated by USP21, we asked whether a curated list of 114 FOXM1 target genes is correlated with USP21 amplification using gene set enrichment analysis (GSEA). This analysis revealed strong enrichment for the FOXM1 transcriptional network in USP21-amplified breast cancers (Table S1).

USP21 Affects Paclitaxel Response in BLBC

In addition to its role in cancer proliferation, high FOXM1 expression has been attributed to resistance to platinum-based drugs (Zhou et al., 2014) and taxanes (Carr et al., 2010; Zhao et al., 2014) in breast cancer and correlated with metastasis and poor patient outcomes. Having identified FOXM1 as a USP21 substrate, we examined whether USP21 knockdown could increase sensitivity to paclitaxel in a FOXM1-dependent manner. The BLBC cell lines MDA-MB-231 and MDA-MB-468 and SUM149 cells were used to assess viability following 72 h of exposure to DMSO or paclitaxel in control (siFF), FOXM1-depleted (siRNA targeting FOXM1 [siFOXM1]), and USP21-depleted (siUSP21) cells. In addition, in MDA-MB-231 cells, we used a cell line containing a stably integrated, doxycyclineinducible version of FOXM1, allowing us to examine viability in USP21-depleted-FOXM1-induced (siUSP21 + FOXM1b) conditions. Across all cell lines assessed, there is a significant reduction in viability between FOXM1- and USP21-depleted conditions treated with paclitaxel compared with the same depletion condition in which cells were not treated with paclitaxel (DMSO control) (Figure 5A). Therefore, while depletion of USP21 (and FOXM1) impairs proliferation in each of these cell lines under control conditions, there is a statistically significant decrease in viability when USP21 depletion is combined with paclitaxel treatment. Specifically, in MDA-MB-231 cells exposed to paclitaxel, cell viability was reduced by 40.9% and 38.3% compared with control in FOXM1- and USP21-depleted conditions, respectively (Figure 5A, top). However, cell viability is only reduced by 16.7% in cells in which USP21 was depleted but FOXM1 levels are restored with doxycycline induction. In MDA-MB-468 cells treated with paclitaxel, viability was more strongly reduced, by 81.3% and 41.5% compared with control in FOXM1- and USP21-depleted conditions, respectively (Figure 5A, middle). Finally, in SUM149 cells treated with paclitaxel, viability was significantly reduced, by 43.6% and 20.2% in FOXM1- and USP21-depleted conditions, respectively (Figure 5A, bottom). This is particularly striking

considering that SUM149 cells do not show a significant reduction in viability when treated with paclitaxel alone. The significant difference in cell viability resulting from FOXM1 depletion and USP21 depletion combined with a significant rescue of viability when FOXM1 is overexpressed in the USP21-depleted conditions suggests that FOXM1 significantly contributes to paclitaxel sensitivity and is a critical USP21 substrate, although perhaps not the only one, contributing to the differences in paclitaxel sensitivity observed in USP21-depleted cells.

Based on the realization that USP21 depletion sensitizes cells to paclitaxel, we next determined how BLBC cells would respond to paclitaxel following USP21 depletion in a mouse xenograft model. SUM149 is a BLBC cell line that is paclitaxel insensitive in mouse xenografts (Figure 5B, red line). SUM149 cells were transduced with lentivirus expressing scrambled short hairpin RNA (shRNA) (shControl) or shRNA targeting USP21 (shUSP21) and implanted in the mammary fat pads of non-obese diabetic (NOD)-severe combined immunodeficiency (SCID) gamma mice following selection for infected cells (Figure S5C). Mice were then administered either paclitaxel (10 mg/kg of body weight) or vehicle twice weekly, and tumor volume was monitored twice weekly for six weeks. The results revealed that average tumor volume was reduced from 1,101.75 mm^3 in the control condition to 414 mm^3 (a 62.4% reduction) over six weeks because of depletion of USP21 and exposure to paclitaxel (Figure 5B, blue line). These results suggest that inhibition of USP21 may provide a therapeutic benefit in BLBC by antagonizing proliferation and enhancing chemotherapy resistance effects driven by FOXM1 activation.

DISCUSSION

Here, we identify the transcription factor FOXM1 as a substrate of the DUB USP21. USP21 stabilizes FOXM1, and suppressing USP21 reduces FOXM1 abundance, which subsequently downregulates the FOXM1 transcriptional network. This leads to a mitotic entry delay, slowed proliferation, and sensitivity to paclitaxel, both in culture and in animal xenografts. Phenotypes linked to USP21 depletion were partially mitigated by forced expression of FOXM1. This suggests that FOXM1 is a key USP21 substrate with respect to these phenotypes but likely is not the only target determining the role of USP21 in the cell cycle, cancer proliferation, and paclitaxel sensitivity. Nevertheless, we predict that targeting USP21 could have therapeutic potential in aggressive cancers marked by high FOXM1 expression and with concordant genome instability.

To date, few USP21 substrates have been identified. Many validated substrates, including GATA3 (Zhang et al., 2013), GLI1 (Heride et al., 2016), NANOG (Jin et al., 2016), and ubiquitinated histone H2A K119 (Nakagawa et al., 2008), are either transcription factors or involved in the regulation of transcription. Our identification of FOXM1, a transcription factor that regulates cell cycle progression, as a USP21 substrate supports this theme. Given these roles, it is interesting to consider USP21 as a general transcriptional regulator through its dual function in stabilizing transcription factors and creating a permissive landscape for transcription to occur through the removal of ubiquitin at H2A K119, a post-translational modification associated with transcriptional repression. Future work integrating these

aspects of transcription under the control of USP21 may underscore its importance in the promotion of transcriptional activity.

BLBC is characterized by high genomic instability, which contributes to a distinctive pattern of CNA gains at 1q, 6p, 8q, and 10p, along with frequent losses at 4p, 5q, 14q, and 15q (Adélaïde et al., 2007). Outside of *TP53* loss, which occurs in more than 80% of cases, there are few mutations in well-characterized oncogenes or additional tumor suppressors linked to BLBC. The *USP21* genomic location is 1q23, an amplified region suggested to contain putative driver genes for the BLBC subtype (Silva et al., 2015). The *FOXM1* genomic location is 12p13, another amplified region associated with the BLBC subtype. Our analysis supports links of *FOXM1* expression, the BLBC subtype, and proliferation, as well as a correlation between *USP21* expression at the genomic and transcriptional levels (Figure 4B) and a correlation between USP21 and FOXM1 levels in BLBC. We show that USP21 amplification correlates with proliferation score of the tumor. While this result is partially complicated by amplification of 1q and particularly the USP21 genomic locus, being enriched in aggressive BLBC-subtyped tumors (Silva et al., 2015), this points to its potential role in disease. The evidence presented here suggests that USP21 could act as a proliferative driver by promoting FOXM1 stability and transcriptional function, which promotes proliferation in BLBC with amplified USP21 and FOXM1 expression. We speculate that increased gene dosage of USP21 contributes to the proliferative features of BLBC and that it likely acts coordinately with additional proliferative drivers on 1q, as well as with other genes located within recurrently altered genomic regions.

Because of its myriad roles in the promotion and maintenance of cancer, FOXM1 has garnered significant attention as a target for therapeutic intervention (Halasi and Gartel, 2013b). Because FOXM1 is recurrently activated in specific disease subtypes, including most BLBC and high-grade serous ovarian cancers, the rationale, therapeutic window, and patient numbers exist to support its therapeutic candidacy. Moreover, while therapies that target specific transcription factors are clinically effective, including hormone therapy in breast cancer and all-*trans* retinoic acid (ATRA) in acute promyelocytic leukemia (Bradner et al., 2017), in most cases, transcription factors have defied efforts aimed at chemical inhibition (e.g., c-Myc).

Here, we provide the rationale for an indirect method of down-regulating FOXM1 activity through the inhibition of USP21. In contrast with transcription factors, DUBs have favorable properties that make them attractive therapeutic targets. More specifically, USP-family DUBs have deep, active pockets relying on a catalytic triad (Komander et al., 2009) that is generally tractable with small-molecule inhibitors (Shi and Grossman, 2010). The identification of potent and highly selective USP7 inhibitors has brought to the forefront the chemical tractability of DUBs as a therapeutic class (Kategaya et al., 2017; Turnbull et al., 2017). The crystal structure of the USP21 catalytic core has been solved (Ye et al., 2011), which facilitates the identification and development of potent and highly selective small-molecule inhibitors through structure-activity relationship studies. Future work describing additional substrates and processes influenced by USP21 may uncover additional examples in which USP21 inhibition may demonstrate therapeutic benefit.

STAR★METHODS

Detailed methods are provided in the online version of this paper and include the following:

CONTACT FOR REAGENT AND RESOURCE SHARING

Further information and requests for resources and reagents should be directed to and will be fulfilled by the Lead Contact, Michael J. Emanuele (emanuele@email.unc.edu).

EXPERIMENTAL MODEL AND SUBJECT DETAILS

Cell Lines—293T, HeLa, MDA-MB-231, MDA-MB-468, HMEC, MCF7, MCF10A and BT474 cells were all obtained from the American Type Culture Collection (ATCC). SUM149 and SUM159 cells were obtained from BioIVT (formerly Astrand). All cell lines are female.

Mouse Model—All mouse studies were conducted following an Institute of Animal Care and Use Committee (IACUC)-approved protocol. BALB/c female nude mice (nu/nu) bread by the UNC-Chapel Hill Mouse Phase 1 Unit (MP1U) were used at 8 weeks of age, housed four per cage and provided sterilized pellet chow and given tap water *ad libitum*. Animal rooms are maintained at 22°C and lighted 16 hours per day.

METHOD DETAILS

Cell Culture—Cell lines were all obtained from the American Type Culture Collection, or BioIVT. 293T, HeLa, MDA-MB-231, MDA-MB-468, HMEC, MCF7, MCF10A, SUM159, and BT474 cells were cultured in Dulbecco's modified Eagle's medium (DMEM; GIBCO) supplemented with 10% FBS (Atlanta Biologicals) and 1% Pen/Strep (GIBCO). SUM149 cells were obtained from BioIVT and cultured in either F-12 medium (GIBCO) supplemented with 5% FBS (Atlanta Biologicals), 10mM HEPES pH7.5, 1μg/mL hydrocortisone, 5μg/mL insulin (GIBCO) and 1% Pen/Strep (GIBCO) or in HuMEC Ready Medium (GIBCO). All cells were incubated at 37°C and 5% CO_2.

Transfections and Treatments—All siRNA transfections were performed using Lipofectamine RNAiMAX (ThermoFisher) following instructions in the manufacturer's instructions. Sequence of siRNAs used in this study are described in Table S2. All plasmid transfections into 293T cells were performed using Mirus TransIT-293 reagent (Mirus Bio) following instructions in the manufacturer's protocol. Plasmid transfections into other cell lines were performed using Lipofectamine 2000 (ThermoFisher) according to manufacturer's instructions. PR-619 and MG132 (Selleck Chemicals) were used at a concentration of 10μM for 8 hours and 6 hours, respectively. Cycloheximide (MilliporeSigma) was used at a concentration of 100ng/mL for the indicated time.

Molecular Cloning—pDEST-HA-FOXM1b, pDEST-Myc-USP21, pDEST-FLAG-FOXM1b, pINDUCER20-FOXM1b and pINDUCER20 USP21 were all generated using Gateway Cloning Technology (ThermoFisher) from pDONR223-FOXM1b and pDONR223-USP21 plasmids. All FOXM1 fragments described in Figure S1 were ordered as synthetic gene fragments (IDT) and subsequently cloned into pDONR223 and pDEST-Myc plasmids

for expression using Gateway Cloning Technology. The FOXM1 6x-DBE luciferase reporter plasmid was a gift from Michael Whitfield (Dartmouth Univsersity). FLAG-HA-USP21 plasmid was a gift from Wade Harper (Addgene plasmid # 22574) (Sowa et al., 2009). pINDUCER20 was a gift from Stephen Elledge (Addgene plasmid # 44012) (Meerbrey et al., 2011). 6-HIS-FLAG Ubiquitin plasmid was a gift from Philippe Soubeyran. Site-directed mutagenesis with QuickChange Lightning Kit (Agilent) was used to generate C221A MSCV-FLAG-HA-USP21 following manufacturer's instructions. Primers used are described in Table S2.

Lentivirus Production—293T cells were transfected with pINDUCER20 plasmids mixed with VSV-G, Gag-Pol, Tat and Rev lentivirus packaging helper plasmids in a 1:4 ratio. Media containing viral particles was harvested 24 and 48 hours later, passed through a 0.45μM filter and stored frozen at −80°C. MDA-MB-231 cells were transduced with lentiviral particles and selected with G418 to isolate successfully transduced cells.

Immunoblotting—Samples were lysed in RIPA buffer (150mM NaCl, 50mM Tris pH 7.5, 5mM EDTA, 1% NP-40, 0.5% sodium deoxycholate, 0.1% SDS) supplemented with 1μg/mL aprotinin and leupeptin, 10μg/mL leupeptin, 1mM sodium orthovanadate, 1mM NaF, and 1mM AEBSF. Protein concentration was quantified by Pierce BCA assay (ThermoFisher) and samples were prepared by boiling in Laemmli buffer for 5 minutes. Samples were separated by gel electrophoresis using homemade or TGX (Bio-Rad) SDS-PAGE gels and transferred to nitrocellulose membrane. All blocking and antibody washing steps were performed in 5% nonfat dried milk (Bio-Rad) diluted in TBS-T (137mM NaCl, 2.7mM KCl, 25mM Tris pH 7.4, 1% Tween-20). All primary antibody incubations were performed shaking at 4°C for 16 hours. All secondary antibody incubations were performed shaking at room temperature for 1 hour. All washing steps were performed using TBS-T. Protein abundance was visualized by chemiluminescence using Pierce ECL (ThermoFisher), or Clarity ECL (Bio-Rad). A list of all antibodies used in this study are described is Table S2.

Immunoprecipitations—293T cells were transfected with the indicated plasmids and lysed in NETN buffer (100mM NaCl, 20mM Tris pH 8, 0.5mM EDTA, 0.5% NP-40 supplemented with 1μg/mL aprotinin and leupeptin, 10μg/mL leupeptin, 1mM sodium orthovanadate, 1mM NaF, and 1mM AEBSF) 48 hours after transfection. 1μg of the indicated antibody was conjugated to a 50μl mix of magnetic Protein A and Protein G beads (Bio-Rad) at room temperature for 1 hour. 1mg of lysate from each sample was pre-cleared to remove non-specific interactions with a similar volume of Protein A/G beads rotating at 4°C for 1 hour. Following antibody conjugation and pre-clearing, lysate and beads were combined rotating at 4°C for 4 hours. Beads were subjected to multiple rounds of washing with NETN. Proteins were eluted by boiling beads in Laemmli buffer for 10 minutes and visualized by IB.

FOXM1 and USP21 *In Vitro* Binding Assay—FOXM1b was subcloned into a pET-28b backbone to create a C-terminal 6X-Histidine tagged clone, transformed into *Escherichia coli* BL21(DE3) cells, grown to an OD_{600} of 0.5, and induced to express with 250μM of

IPTG shaking at 18°C for 16 hours. USP21 was cloned into a pDEST15 backbone using Invitrogen Gateway cloning technology (ThermoFisher) to create a N-terminal GST-tagged clone, transformed into *Escherichia coli* BL21(DE3) cells, grown to an OD_{600} of 0.5, and induced to express with 100μM of IPTG shaking at 25°C for 5 hours. Bacterial pellets were resuspended in 40mL lysis buffer (20mM KH_2PO_4 pH 7.5, 500mM NaCl, 10% glycerol, 2μg/mL aprotinin, 10μg/mL leupeptin, 2μg/mL pepstatin, 1mM sodium orthovanadate, 1mM NaF 1mM AEBSF, 10mg/mL lysozyme, 40U DNase I; leupeptin and AEBSF not included in GST-USP21 lysis). 6HIS-FOXM1b and GST-USP21 were batch purified from crude lysate on His-Pur Ni-NTA resin (ThermoFisher) and glutathione agarose resin (GoldBio) following manufacturer's protocols, respectively. Following elution, proteins were buffer exchanged (25mM Tris pH 7.4, 200mM NaCl, 2mM DTT) using Zeba desalting columns (ThermoFisher) following manufacturer's protocols. For interaction studies, 1mg of GST or GST-USP21 was conjugated to GSH agarose resin rotating at room temperature for 1 hour. Then, 1μg 6HIS-FOXM1b was added and incubation continued with rotation at room temperature for 1 hour. Following three rounds of washing with PBS, protein complexes were eluted (50mM Tris pH 8.0, 10mM glutathione), resuspended in Laemmli buffer and assessed by IB.

FOXM1 Transcriptional Reporter Assay—293T cells were transfected with FOXM1 6x-DBE luciferase reporter and FLAG-HA-USP21 plasmids as indicated and collected 24 hours after transfection. Lysates were prepared according to the protocol described in the Luciferase Assay System (Promega). Measurements were made in a 96-well plate and results represent the average of triplicates for each experiment condition described.

Cell Cycle Progression into Mitosis—MDA-MB-231 cells were transfected with the indicated siRNA using RNAiMAX. 48 hours following transfection, media on cells was refreshed with media containing 2μg/mL aphidicolin. 24 hours later, media on cells was refreshed with media containing 200ng/mL nocodazole. Cells were harvested at the indicated time points and samples were prepared for IB or for flow cytometry by fixation in 70% ethanol. For flow cytometry, cells were blocked for 30 minutes, incubated with rabbit anti-phospho-Histone H3 (S10) antibody for 1 hour, then incubated with goat anti-rabbit Alexa Fluor 488 for 1 hour, and finally stained with 25μg/mL propidium iodide, 100μg/mL RNase A for 1 hour. All blocking, washing, and staining steps were done with 1% BSA in PBS. All samples were run on a CyAn ADP analyzer (Beckman Coulter) and data was analyzed using FlowJo X software.

***In Vitro* Paclitaxel Sensitivity Assays—**MDA-MB-231 pINDUCER20-FOXM1b, MDA-MB-468 and SUM149 cells were transfected with the indicated siRNAs. 24 hours following transfection, cells were seeded in triplicates at a density of 7,500 cells / well in a 96-well plate. 12 hours after seeding, media supplemented with paclitaxel, and in one set of siUSP21 triplicates (MDA-MB-231 pINDUCER20 FOXM1b only), paclitaxel with 10ng/mL doxycycline was added to cells. After a 72-hour incubation, cell viability was assessed using PrestoBlue reagent according to manufacturer's instructions.

Tumor Xenograft—SUM149 cells were transduced with lentivirus expressing shRNA against USP21 or a non-targeting control and selected of positive expression with puromycin. Immediately following selection, orthotopic xenografts were established for all conditions by injecting subcutaneously 5×10^6 cells mixed 50:50 in serum-free media:matrigel into the right mammary fat pad of athymic, female nude mice. Tumor volume was measured with calipers and calculated using the equation Volume = Length × $\text{Width}^2 \times 0.563$. Upon tumors reaching a volume 100mm^3, mice were administered a bi-weekly intraperitoneal injection of 10mg/kg (body weight) paclitaxel or equivalent volume of vehicle. Tumor volume measurements were recorded twice weekly for 6 weeks.

Proliferation Assays—MDA-MB-231 pINDUCER20 FOXM1b and MDA-MB-468 cells were transfected with the indicated siRNA, then 12 hours later, 30,000 cells/well were seeded into 24-well plates in triplicates for each condition. Growth was monitored through phase-contrast imaging using the IncuCYTE Zoom (Essen Bioscience) live-cell imaging device. Images were taken every 6 hours for 120 total hours and growth was calculated for each time point as the average percent confluence of 4 images taken per well. Values were normalized for each respective condition so initial confluence starts at 0%.

HeLa cells were transfected with the indicated siRNA, then 24 hours later, transfected with the indicated plasmids. Growth was monitored using PrestoBlue cell viability reagent (ThermoFisher) following the manufacturers protocol. Measurements were taken in triplicate for each time point with each point described as a percentage of the first measurement taken following seeding.

***In Vivo* Deubiquitination Assay—**The *in vivo* ubiquitination assay was performed as described previously (Bonacci et al., 2014). Briefly, 293T cells were transfected with the indicated plasmids and harvested in PBS 24 hours following transfection. 80% of the cell suspension was lysed in 6M guanidine-HCL buffer and 6HIS-ubiquitinated proteins were captured on HisPur Ni-NTA resin (ThermoFisher) while the remaining 20% of sample was used to prepare inputs. Pull-down eluates and inputs were separated on SDS-PAGE gels and analyzed by immunoblot.

***In Vitro* Deubiquitination Assay—**293T cells were transfected with HA-FOXM1b and 6xHIS-FLAG-Ubiquitin and separately with FLAG-HA-USP21^{WT}, FLAG-$\text{HAUSP21}^{\text{C221A}}$ and empty vector, respectively. 48 hours following transfection, cells transfected with HA-FOXM1b/6xHIS-FLAG-Ubiquitin were treated with complete DMEM supplemented with 25μM MG132 for 1 hour prior to harvesting. HA-FOXM1b/6xHIS-FLAG-Ubiquitin cells were lysed in RIPA buffer (150mM NaCl, 50mM Tris pH 7.5, 5mM EDTA, 1% NP-40, 0.5% sodium deoxycholate, 0.1% SDS) supplemented with 1mg/mL aprotinin and leupeptin, 10mg/mL leupeptin, 1mM sodium orthovanadate, 1mM NaF, 1mM AEBSF and 20mM NEM. FLAG-HA-USP21^{WT}, FLAG-HA-$\text{USP21}^{\text{C221A}}$ and empty vector cells were lysed in RIPA buffer without additional inhibitors. HA-tagged proteins were captured from clarified cell lysate on 50μL EZview Red Anti-HA Affinity Gel (MilliporeSigma) according to manufacturer's instructions. Following capture and washing, beads containing captured HA-FOXM1b/6xHIS-FLAG-ubiquitin were resuspended in DUB Buffer (50mM Tris pH 7.5, 50mM NaCl, 5mM DTT, 5mM $MgCl_2$) and mixed equally with beads resuspended in DUB

buffer containing captured FLAG-HA-USP21^{WT}, FLAG-HA-USP21^{C221A} and empty vector cell lysate. Beads were incubated with rotation at 37°C for 4 hours and proteins were eluted directly from beads with the addition of Laemlli sample buffer and boiling. Ubiquitination status of HA-FOXM1b was assessed by IB as described above.

RT-qPCR—MDA-MB-231 cells were transfected with the indicated siRNA and harvested 72 hours after transfection. RNA was extracted using RNeasy Mini Kit (QIAGEN) following manufacturer's instructions. 1μg of RNA was used to generate cDNA libraries with random primers using SuperScript III Reverse Transcriptase (ThermoFisher) following manufacturer's instructions. Samples were diluted 1:10 and transcript abundance was quantified using SsoAdvanced SYBR Green (Bio-Rad) on a QuantStudio 7 Flex Real-Time PCR system (ThermoFisher) normalized to *GAPDH*, with each condition run in triplicates. Data displayed as the relative quantity of transcript quantified using the 2−ΔΔCt method (Schmittgen and Livak, 2008). All primers used are described in Table S2.

QUANTIFICATION AND STATISTICAL ANALYSIS

TCGA Dataset Analysis—Upper quartile normalized RSEM gene-level data for 1095 invasive breast cancers were downloaded from the legacy TCGA-BRCA project using the NIH Genome Data Commons (https://portal.gdc.cancer.gov/legacy-archive/). Proliferation score was calculated for each sample analyzed as previously described (Nielsen et al., 2010) and compared to log2-transformed, median-centered *FOXM1* expression data for each sample analyzed. FOXM1 transcriptional targets were log2-transformed, median-centered and compared to log2-transformed, median-centered FOXM1 expression. Gene Set Enrichment Analysis (GSEA) (Mootha et al., 2003; Subramanian et al., 2005) was performed for a previously derived FOXM1 target gene list (Chen et al., 2013) comparing USP21-amplified and USP21-non-amplified patient tumors. RPPA normalized data was downloaded from the TCGA PanCanAtlas Publication page (http://api.gdc.cancer.gov/data/fcbb373e-28d4-4818-92f3-601ede3da5e1) and data for 879 breast samples were extracted. GISTIC values were downloaded from Broad's Firehouse (http://gdac.broadinstitute.org/runs/analyses__2016_01_28/data/BRCA-TP/20160128/gdac.broadinstitute.org_BRCA-TP.CopyNumber_Gistic2.Level_4.2016012800.0.0.tar.gz). There were 857 samples with both RPPA and copy number data. GISTIC values of 2 were considered highly amplified for USP1 and compared to those without high amplification of USP21 for volcano plots and to compare proliferation score. An FDR-corrected Wilcoxon rank sum test was used to calculate proteins associated with USP21 copy number status. Data from 505 breast invasive carcinoma samples from TCGA (Cancer Genome Atlas Network, 2012) were downloaded from cBioPortal (http://www.cbioportal.org/) (Cerami et al., 2012; Gao et al., 2013). Percent of samples with CNA amplification and mRNA overexpression (Z-score threshold ± 2) of 92 DUBs was aggregated.

Other Statistical Analysis—Analysis of FOXM1 half-life stability was assessed by densitometry of bands on immunoblots using ImageJ. Band intensity was calculated for FOXM1 and the respective loading control for each lane/time point. Non-specific background was subtracted from the signal of each band. FOXM1 intensity at a given time point was normalized to the amount of loading control in that lane. For calculating half-life,

all time points were calculated as a percentage of initial FOXM1 abundance for each respective condition. The best-fit nonlinear regression curve was drawn through points and half-life was assed as time when y = 50% using GraphPad Prism 6. Key details of the statistical analysis pertaining to RT-qPCR, proliferation assays, paclitaxel sensitivity assays and tumor xenograft assays are described in the corresponding Method Details for those experiments and in the legends for Figures 3B, 3E, 5A, and 5B, respectively.

Supplementary Material

Refer to Web version on PubMed Central for supplementary material.

ACKNOWLEDGMENTS

We acknowledge the UNC Flow Cytometry Core Facility (supported in part by the P30 CA016086 Cancer Center Core Support Grant to the UNC Lineberger Comprehensive Cancer Center). The work done in the Emanuele lab was supported by the UNC University Cancer Research Fund, the Susan G. Komen Foundation (CCR14298820), the NIH (R01GM120309), the American Cancer Society (RSG-18-220-01-TBG), and donations from the Brookside Foundation. K.A.H. is supported by a Susan G. Komen Career Catalyst Grant (CCR16376756).

REFERENCES

Adélaïde J, Finetti P, Bekhouche I, Repellini L, Geneix J, Sircoulomb F, Charafe-Jauffret E, Cervera N, Desplans J, Parzy D, et al. (2007). Integrated profiling of basal and luminal breast cancers. Cancer Res. 67, 11565–11575. [PubMed: 18089785]

Bonacci T, Audebert S, Camoin L, Baudelet E, Bidaut G, Garcia M, Witzel II, Perkins ND, Borg JP, Iovanna JL, and Soubeyran P (2014). Identification of new mechanisms of cellular response to chemotherapy by tracking changes in post-translational modifications by ubiquitin and ubiquitin-like proteins. J. Proteome Res 13, 2478–2494. [PubMed: 24654937]

Bradner JE, Hnisz D, and Young RA (2017). Transcriptional Addiction in Cancer. Cell 168, 629–643. [PubMed: 28187285]

Cancer Genome Atlas Network (2012). Comprehensive molecular portraits of human breast tumours. Nature 490, 61–70. [PubMed: 23000897]

Cancer Genome Atlas Research Network (2011). Integrated genomic analyses of ovarian carcinoma. Nature 474, 609–615. [PubMed: 21720365]

Carr JR, Park HJ, Wang Z, Kiefer MM, and Raychaudhuri P (2010). FoxM1 mediates resistance to herceptin and paclitaxel. Cancer Res. 70, 5054–5063. [PubMed: 20530690]

Cerami E, Gao J, Dogrusoz U, Gross BE, Sumer SO, Aksoy BA, Jacobsen A, Byrne CJ, Heuer ML, Larsson E, et al. (2012). The cBio cancer genomics portal: an open platform for exploring multidimensional cancer genomics data. Cancer Discov. 2, 401–404. [PubMed: 22588877]

Chen X, Müller GA, Quaas M, Fischer M, Han N, Stutchbury B, Sharrocks AD, and Engeland K (2013). The forkhead transcription factor FOXM1 controls cell cycle-dependent gene expression through an atypical chromatin binding mechanism. Mol. Cell. Biol 33, 227–236. [PubMed: 23109430]

Chen Y, Li Y, Xue J, Gong A, Yu G, Zhou A, Lin K, Zhang S, Zhang N, Gottardi CJ, and Huang S (2016). Wnt-induced deubiquitination FoxM1 ensures nucleus β-catenin transactivation. EMBO J. 35, 668–684. [PubMed: 26912724]

Fischer M, Grossmann P, Padi M, and DeCaprio JA (2016). Integration of TP53, DREAM, MMB-FOXM1 and RB-E2F target gene analyses identifies cell cycle gene regulatory networks. Nucleic Acids Res. 44, 6070–6086. [PubMed: 27280975]

Fu Z, Malureanu L, Huang J, Wang W, Li H, van Deursen JM, Tindall DJ, and Chen J (2008). Plk1-dependent phosphorylation of FoxM1 regulates a transcriptional programme required for mitotic progression. Nat. Cell Biol 10, 1076–1082. [PubMed: 19160488]

Furuyama T, Nakazawa T, Nakano I, and Mori N (2000). Identification of the differential distribution patterns of mRNAs and consensus binding sequences for mouse DAF-16 homologues. Biochem. J 349, 629–634. [PubMed: 10880363]

Gao J, Aksoy BA, Dogrusoz U, Dresdner G, Gross B, Sumer SO, Sun Y, Jacobsen A, Sinha R, Larsson E, et al. (2013). Integrative analysis of complex cancer genomics and clinical profiles using the cBioPortal. Sci. Signal 6, pl1. [PubMed: 23550210]

Golson ML, and Kaestner KH (2016). Fox transcription factors: from development to disease. Development 143, 4558–4570. [PubMed: 27965437]

Grant GD, Brooks L, 3rd, Zhang X, Mahoney JM, Martyanov V, Wood TA, Sherlock G, Cheng C, and Whitfield ML (2013). Identification of cell cycle-regulated genes periodically expressed in U2OS cells and their regulation by FOXM1 and E2F transcription factors. Mol. Biol. Cell 24, 3634–3650. [PubMed: 24109597]

Halasi M, and Gartel AL (2013a). FOX(M1) news—it is cancer. Mol. Cancer Ther 12, 245–254. [PubMed: 23443798]

Halasi M, and Gartel AL (2013b). Targeting FOXM1 in cancer. Biochem. Pharmacol 85, 644–652. [PubMed: 23103567]

Hannenhalli S, and Kaestner KH (2009). The evolution of Fox genes and their role in development and disease. Nat. Rev. Genet 10, 233–240. [PubMed: 19274050]

Heride C, Rigden DJ, Bertsoulaki E, Cucchi D, De Smaele E, Clague MJ, and Urbé S (2016). The centrosomal deubiquitylase USP21 regulates Gli1 transcriptional activity and stability. J. Cell Sci 129, 4001–4013. [PubMed: 27621083]

Hoadley KA, Yau C, Wolf DM, Cherniack AD, Tamborero D, Ng S, Leiserson MDM, Niu B, McLellan MD, Uzunangelov V, et al.; Cancer Genome Atlas Research Network (2014). Multiplatform analysis of 12 cancer types reveals molecular classification within and across tissues of origin. Cell 158, 929–944. [PubMed: 25109877]

Jeffery JM, Kalimutho M, Johansson P, Cardenas DG, Kumar R, and Khanna KK (2017). FBXO31 protects against genomic instability by capping FOXM1 levels at the G2/M transition. Oncogene 36, 1012–1022. [PubMed: 27568981]

Jin J, Liu J, Chen C, Liu Z, Jiang C, Chu H, Pan W, Wang X, Zhang L, Li B, et al. (2016). The deubiquitinase USP21 maintains the stemness of mouse embryonic stem cells via stabilization of Nanog. Nat. Commun 7, 13594. [PubMed: 27886188]

Kalin TV, Wang IC, Ackerson TJ, Major ML, Detrisac CJ, Kalinichenko VV, Lyubimov A, and Costa RH (2006). Increased levels of the FoxM1 transcription factor accelerate development and progression of prostate carcinomas in both TRAMP and LADY transgenic mice. Cancer Res. 66, 1712–1720. [PubMed: 16452231]

Kategaya L, Di Lello P, Rougé L, Pastor R, Clark KR, Drummond J, Kleinheinz T, Lin E, Upton J-P, Prakash S, et al. (2017). USP7 small-molecule inhibitors interfere with ubiquitin binding. Nature 550, 534–538. [PubMed: 29045385]

Kim I-M, Ackerson T, Ramakrishna S, Tretiakova M, Wang I-C, Kalin TV, Major ML, Gusarova GA, Yoder HM, Costa RH, and Kalinichenko VV (2006). The Forkhead Box m1 transcription factor stimulates the proliferation of tumor cells during development of lung cancer. Cancer Res. 66, 2153–2161. [PubMed: 16489016]

Komander D, Clague MJ, and Urbé S (2009). Breaking the chains: structure and function of the deubiquitinases. Nat. Rev. Mol. Cell Biol 10, 550–563. [PubMed: 19626045]

Kongsema M, Zona S, Karunarathna U, Cabrera E, Man EPS, Yao S, Shibakawa A, Khoo U-S, Medema RH, Freire R, and Lam EW-F (2016). RNF168 cooperates with RNF8 to mediate FOXM1 ubiquitination and degradation in breast cancer epirubicin treatment. Oncogenesis 5, e252. [PubMed: 27526106]

Korver W, Roose J, Wilson A, and Clevers H (1997). The winged-helix transcription factor Trident is expressed in actively dividing lymphocytes. Immunobiology 198, 157–161. [PubMed: 9442387]

Laoukili J, Kooistra MRH, Brás A, Kauw J, Kerkhoven RM, Morrison A, Clevers H, and Medema RH (2005). FoxM1 is required for execution of the mitotic programme and chromosome stability. Nat. Cell Biol 7, 126–136. [PubMed: 15654331]

Laoukili J, Alvarez-Fernandez M, Stahl M, and Medema RH (2008a). FoxM1 is degraded at mitotic exit in a Cdh1-dependent manner. Cell Cycle 7, 2720–2726. [PubMed: 18758239]

Laoukili J, Alvarez M, Meijer LA, Stahl M, Mohammed S, Kleij L, Heck AJ, and Medema RH (2008b). Activation of FoxM1 during G2 requires cyclin A/Cdk-dependent relief of autorepression by the FoxM1 N-terminal domain. Mol. Cell. Biol 28, 3076–3087. [PubMed: 18285455]

Liu M, Dai B, Kang SH, Ban K, Huang FJ, Lang FF, Aldape KD, Xie TX, Pelloski CE, Xie K, et al. (2006). FoxM1B is overexpressed in human glioblastomas and critically regulates the tumorigenicity of glioma cells. Cancer Res. 66, 3593–3602. [PubMed: 16585184]

Major ML, Lepe R, and Costa RH (2004). Forkhead box M1B transcriptional activity requires binding of Cdk-cyclin complexes for phosphorylation-dependent recruitment of p300/CBP coactivators. Mol. Cell. Biol 24, 2649–2661. [PubMed: 15024056]

Meerbrey KL, Hu G, Kessler JD, Roarty K, Li MZ, Fang JE, Herschkowitz JI, Burrows AE, Ciccia A, Sun T, et al. (2011). The pINDUCER lentiviral toolkit for inducible RNA interference *in vitro* and *in vivo*. Proc. Natl. Acad. Sci. USA 108, 3665–3670. [PubMed: 21307310]

Mootha VK, Lindgren CM, Eriksson KF, Subramanian A, Sihag S, Lehar J, Puigserver P, Carlsson E, Ridderstråle M, Laurila E, et al. (2003). PGC-1alpha-responsive genes involved in oxidative phosphorylation are coordinately downregulated in human diabetes. Nat. Genet 34, 267–273. [PubMed: 12808457]

Myatt SS, and Lam EW-F (2007). The emerging roles of forkhead box (Fox) proteins in cancer. Nat. Rev. Cancer 7, 847–859. [PubMed: 17943136]

Myatt SS, Kongsema M, Man CW, Kelly DJ, Gomes AR, Khongkow P, Karunarathna U, Zona S, Langer JK, Dunsby CW, et al. (2014). SUMOylation inhibits FOXM1 activity and delays mitotic transition. Oncogene 33, 4316–4329. [PubMed: 24362530]

Nakagawa T, Kajitani T, Togo S, Masuko N, Ohdan H, Hishikawa Y, Koji T, Matsuyama T, Ikura T, Muramatsu M, and Ito T (2008). Deubiquitylation of histone H2A activates transcriptional initiation via trans-histone cross-talk with H3K4 di- and trimethylation. Genes Dev. 22, 37–49. [PubMed: 18172164]

Nielsen TO, Parker JS, Leung S, Voduc D, Ebbert M, Vickery T, Davies SR, Snider J, Stijleman IJ, Reed J, et al. (2010). A comparison of PAM50 intrinsic subtyping with immunohistochemistry and clinical prognostic factors in tamoxifen-treated estrogen receptor-positive breast cancer. Clin. Cancer Res 16, 5222–5232. [PubMed: 20837693]

Park HJ, Costa RH, Lau LF, Tyner AL, and Raychaudhuri P (2008). Anaphase-promoting complex/cyclosome-CDH1-mediated proteolysis of the forkhead box M1 transcription factor is critical for regulated entry into S phase. Mol. Cell. Biol 28, 5162–5171. [PubMed: 18573889]

Perou CM, Sørlie T, Eisen MB, van de Rijn M, Jeffrey SS, Rees CA, Pollack JR, Ross DT, Johnsen H, Akslen LA, et al. (2000). Molecular portraits of human breast tumours. Nature 406, 747–752. [PubMed: 10963602]

Sadasivam S, Duan S, and DeCaprio JA (2012). The MuvB complex sequentially recruits B-Myb and FoxM1 to promote mitotic gene expression. Genes Dev. 26, 474–489. [PubMed: 22391450]

Schimmel J, Eifler K, Sigurðsson JO, Cuijpers SAG, Hendriks IA, Verlaan-de Vries M, Kelstrup CD, Francavilla C, Medema RH, Olsen JV, and Vertegaal ACO (2014). Uncovering SUMOylation dynamics during cell-cycle progression reveals FoxM1 as a key mitotic SUMO target protein. Mol. Cell 53, 1053–1066. [PubMed: 24582501]

Schmittgen TD, and Livak KJ (2008). Analyzing real-time PCR data by the comparative C(T) method. Nat. Protoc 3, 1101–1108. [PubMed: 18546601]

Shi D, and Grossman SR (2010). Ubiquitin becomes ubiquitous in cancer: emerging roles of ubiquitin ligases and deubiquitinases in tumorigenesis and as therapeutic targets. Cancer Biol. Ther 10, 737–747. [PubMed: 20930542]

Silva GO, He X, Parker JS, Gatza ML, Carey LA, Hou JP, Moulder SL, Marcom PK, Ma J, Rosen JM, and Perou CM (2015). Cross-species DNA copy number analyses identifies multiple 1q21-q23 subtype-specific driver genes for breast cancer. Breast Cancer Res. Treat 152, 347–356. [PubMed: 26109346]

Sorlie T, Tibshirani R, Parker J, Hastie T, Marron JS, Nobel A, Deng S, Johnsen H, Pesich R, Geisler S, et al. (2003). Repeated observation of breast tumor subtypes in independent gene expression data sets. Proc. Natl. Acad. Sci. USA 100, 8418–8423. [PubMed: 12829800]

Sowa ME, Bennett EJ, Gygi SP, and Harper JW (2009). Defining the human deubiquitinating enzyme interaction landscape. Cell 138, 389–403. [PubMed: 19615732]

Subramanian A, Tamayo P, Mootha VK, Mukherjee S, Ebert BL, Gillette MA, Paulovich A, Pomeroy SL, Golub TR, Lander ES, and Mesirov JP (2005). Gene set enrichment analysis: a knowledge-based approach for interpreting genome-wide expression profiles. Proc. Natl. Acad. Sci. USA 102, 15545–15550. [PubMed: 16199517]

Turnbull AP, Ioannidis S, Krajewski WW, Pinto-Fernandez A, Heride C, Martin ACL, Tonkin LM, Townsend EC, Buker SM, Lancia DR, et al. (2017). Molecular basis of USP7 inhibition by selective small-molecule inhibitors. Nature 550, 481–486. [PubMed: 29045389]

Wang X, Arceci A, Bird K, Mills CA, Choudhury R, Kernan JL, Zhou C, Bae-Jump V, Bowers A, and Emanuele MJ (2017). VprBP/DCAF1 Regulates the Degradation and Nonproteolytic Activation of the Cell Cycle Transcription Factor FoxM1. Mol. Cell. Biol 37, e00609–16. [PubMed: 28416635]

Weigman VJ, Chao H-H, Shabalin AA, He X, Parker JS, Nordgard SH, Grushko T, Huo D, Nwachukwu C, Nobel A, et al. (2012). Basal-like Breast cancer DNA copy number losses identify genes involved in genomic instability, response to therapy, and patient survival. Breast Cancer Res. Treat 133, 865–880. [PubMed: 22048815]

Yang H, He X, Zheng Y, Feng W, Xia X, Yu X, and Lin Z (2014). Down-regulation of asparagine synthetase induces cell cycle arrest and inhibits cell proliferation of breast cancer. Chem. Biol. Drug Des 84, 578–584. [PubMed: 24775638]

Ye Y, Akutsu M, Reyes-Turcu F, Enchev RI, Wilkinson KD, and Komander D (2011). Polyubiquitin binding and cross-reactivity in the USP domain deubiquitinase USP21. EMBO Rep. 12, 350–357. [PubMed: 21399617]

Zhang J, Chen C, Hou X, Gao Y, Lin F, Yang J, Gao Z, Pan L, Tao L, Wen C, et al. (2013). Identification of the E3 deubiquitinase ubiquitin-specific peptidase 21 (USP21) as a positive regulator of the transcription factor GATA3. J. Biol. Chem 288, 9373–9382. [PubMed: 23395819]

Zhao F, Siu MKY, Jiang L, Tam KF, Ngan HYS, Le XF, Wong OGW, Wong ESY, Gomes AR, Bella L, et al. (2014). Overexpression of forkhead box protein M1 (FOXM1) in ovarian cancer correlates with poor patient survival and contributes to paclitaxel resistance. PLoS ONE 9, e113478. [PubMed: 25411964]

Zhou J, Wang Y, Wang Y, Yin X, He Y, Chen L, Wang W, Liu T, and Di W (2014). FOXM1 modulates cisplatin sensitivity by regulating EXO1 in ovarian cancer. PLoS ONE 9, e96989. [PubMed: 24824601]

Highlights

- Cell cycle transcription factor FOXM1 is activated in basal-like breast cancer
- USP21 deubiquitinates FOXM1 via a direct enzyme-substrate relationship
- USP21 promotes cell cycle and paclitaxel resistance in basal-like breast cancer
- USP21 is recurrently overexpressed and represents a potential therapeutic target

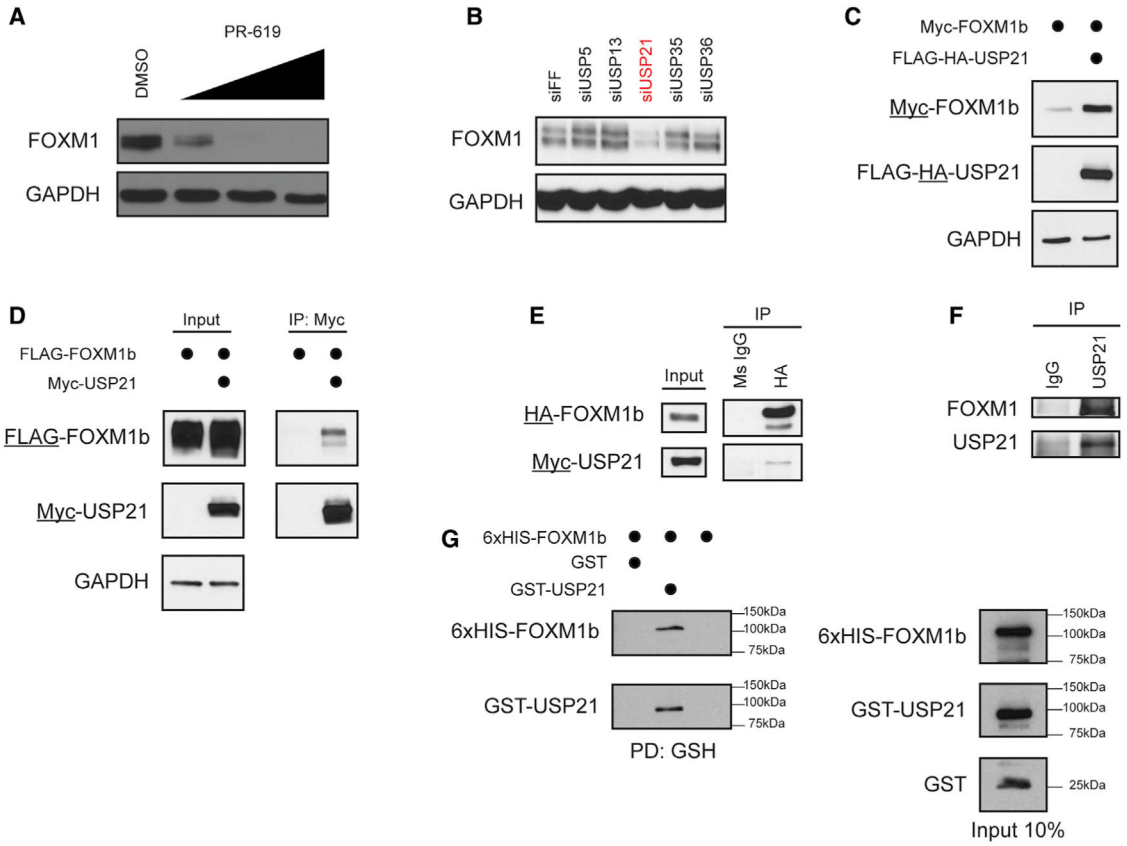

Figure 1. USP21 Binds and Regulates FOXM1 Abundance

(A) HeLa cells treated with vehicle or 2.5, 5, or 10 mM PR-619 for 8 h were analyzed by immunoblot (IB).

(B) HeLa cells were transfected with a pool of four siRNAs targeting respective DUBs. FOXM1 stability was assessed by IB 72 h after transfection.

(C) FOXM1 levels were assessed by IB following transfection of Myc-FOXM1b and FLAG-HA-USP21 in 293T cells 48 h after transfection.

(D) FLAG-FOXM1b and Myc-USP21 were co-expressed in 293T cells. Protein complexes were immunopurified with anti-Myc and analyzed by IB.

(E) HA-FOXM1b and Myc-USP21 were co-expressed in 293T cells. Lysates were immunopurified with anti-mouse immunoglobulin G (IgG) or anti-HA and analyzed by IB.

(F) Endogenous USP21 was immunopurified from HeLa whole-cell lysates and analyzed by IB.

(G) Recombinant 6xHIS-FOXM1b was incubated with recombinant GST-USP21. Complexes were captured on glutathione (GSH) agarose beads and analyzed by IB.

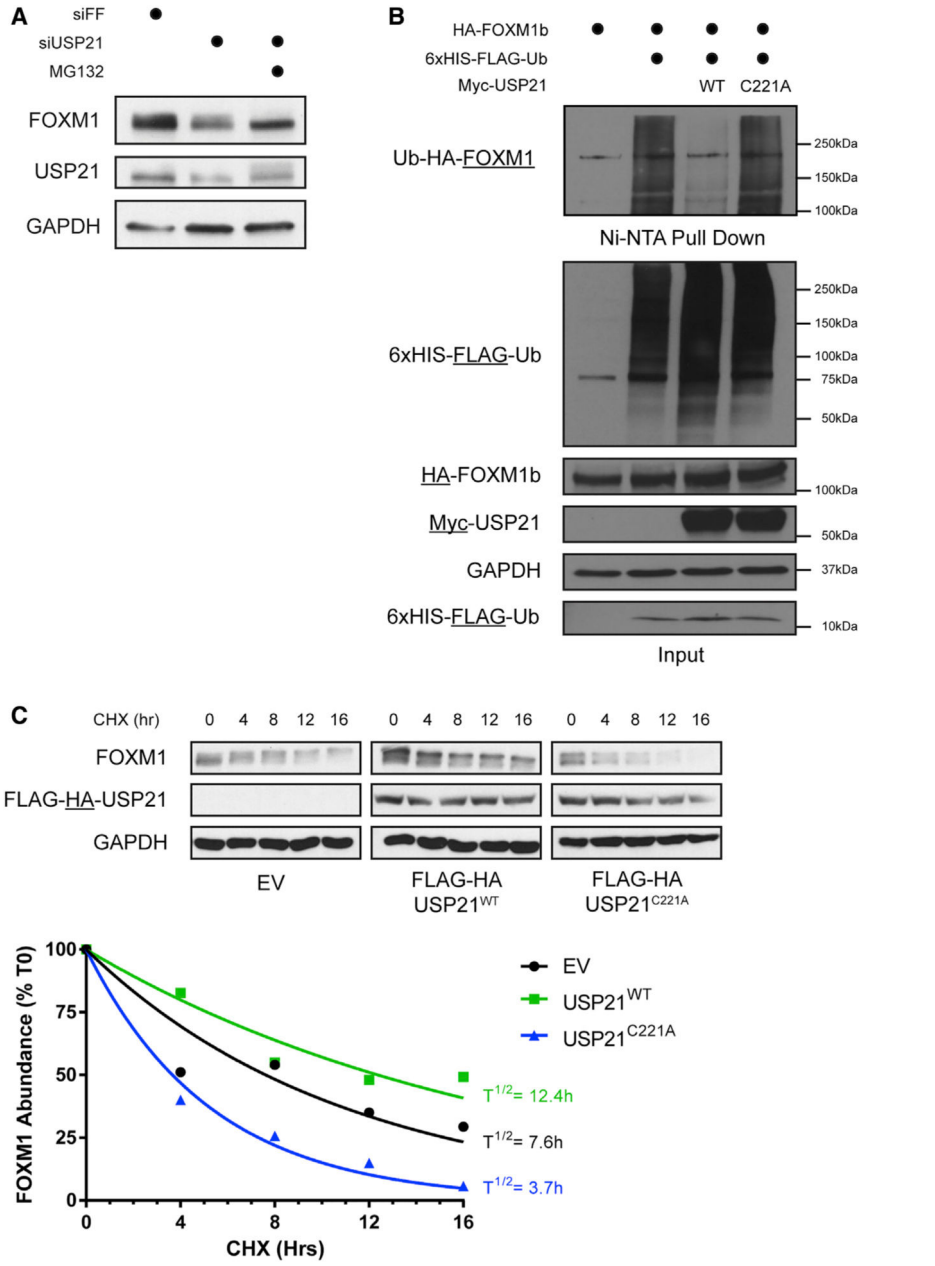

Figure 2. USP21 Protects FOXM1 from Proteasomal Degradation

(A) HeLa cells were transfected with the indicated siRNAs. After 48 h, HeLa cells were treated with 10 μM MG132 or vehicle for 6 h.

(B) 293T cells transfected with the indicated plasmids were lysed under denaturing conditions and subjected to Ni-NTA pull-down. The ubiquitination status of FOXM1 in each condition was assessed by IB.

(C) Top: 293T cells were transfected with the indicated plasmids. After 48 h, 100 ng/mL of cycloheximide was added to the cells and samples were taken every 4 h for 16 h. Bottom: densitometry analysis performed on corresponding IBs to assess FOXM1 half-life in the indicated conditions.

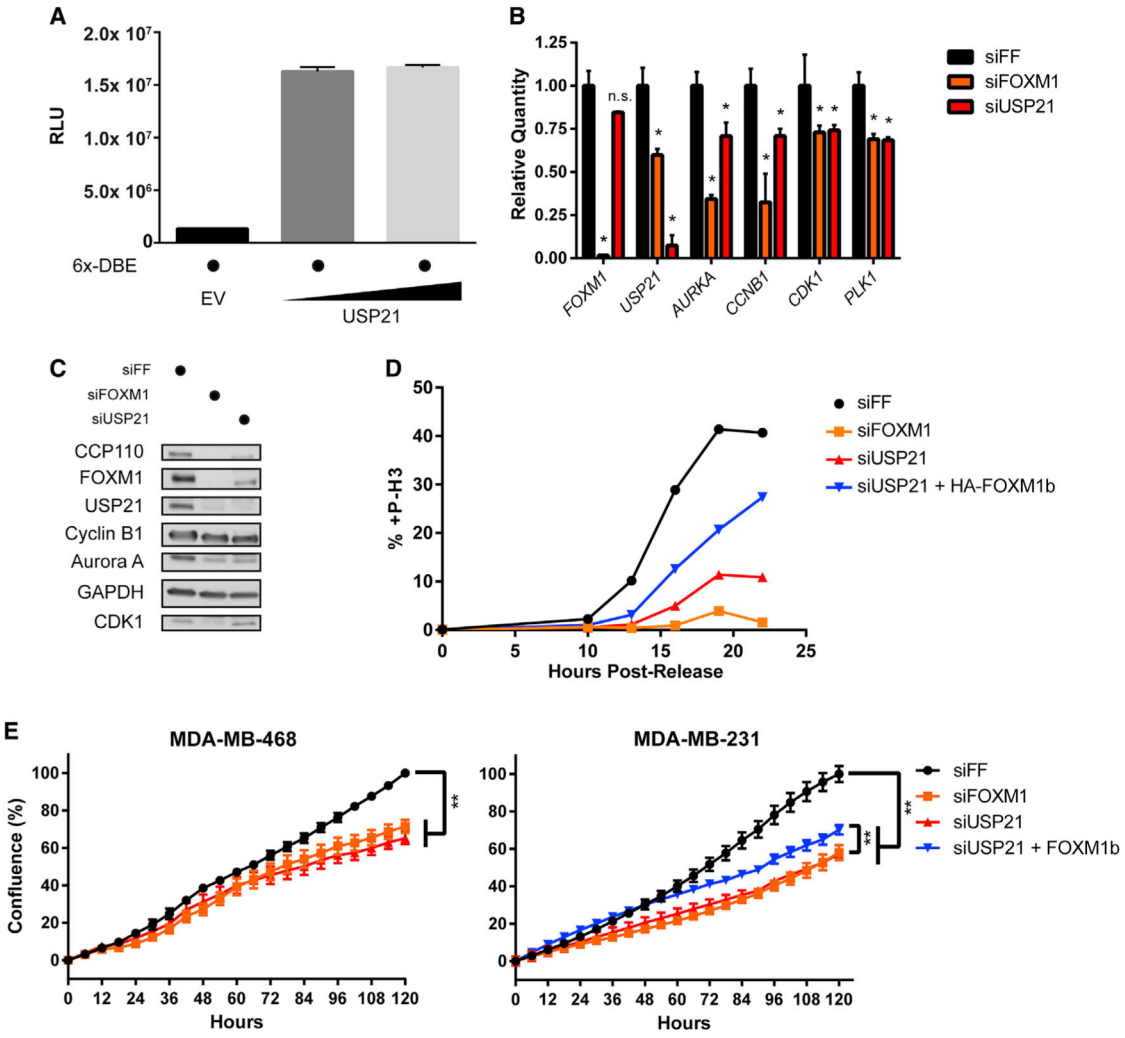

Figure 3. USP21 Affects Growth through Modulation of the FOXM1 Transcriptional Network

(A) FOXM1 transcriptional activity was measured by quantifying luciferase activity in 293T cells expressing the 6x-DBE FOXM1 luciferase reporter with and without USP21 overexpression. Error bars represent SEM.

(B) Relative abundance of FOXM1 target transcripts was assessed by RT-qPCR following RNA extraction from MDA-MB-231 cells transfected with the indicated siRNA for 72 h. Each condition represents means of triplicates. Error bars represent min-max. *p ≤ 0.05 based on Student's t test performed on ΔCt values.

(C) IB of cells used in (B) showing protein levels of various FOXM1 targets.

(D) Mitosis was scored by measuring P-H3-positive cells by flow cytometry in MDA-MB-231 cells transfected with the indicated siRNA or plasmids following release from aphidicolin synchronization at the indicated times.

(E) Growth was measured as the percentage of confluence in the dish every 6 h over 120 h in MDA-MB-468 (left) and MDA-MB-231 pINDUCER20 FOXM1b cells (right) treated with the indicated siRNAs (or 10 ng/mL of doxycycline) using the IncuCyte live-cell imaging system. Each point represents mean of triplicates. Error bars represent SEM. **p ≤ 0.01 based on linear regression analysis.

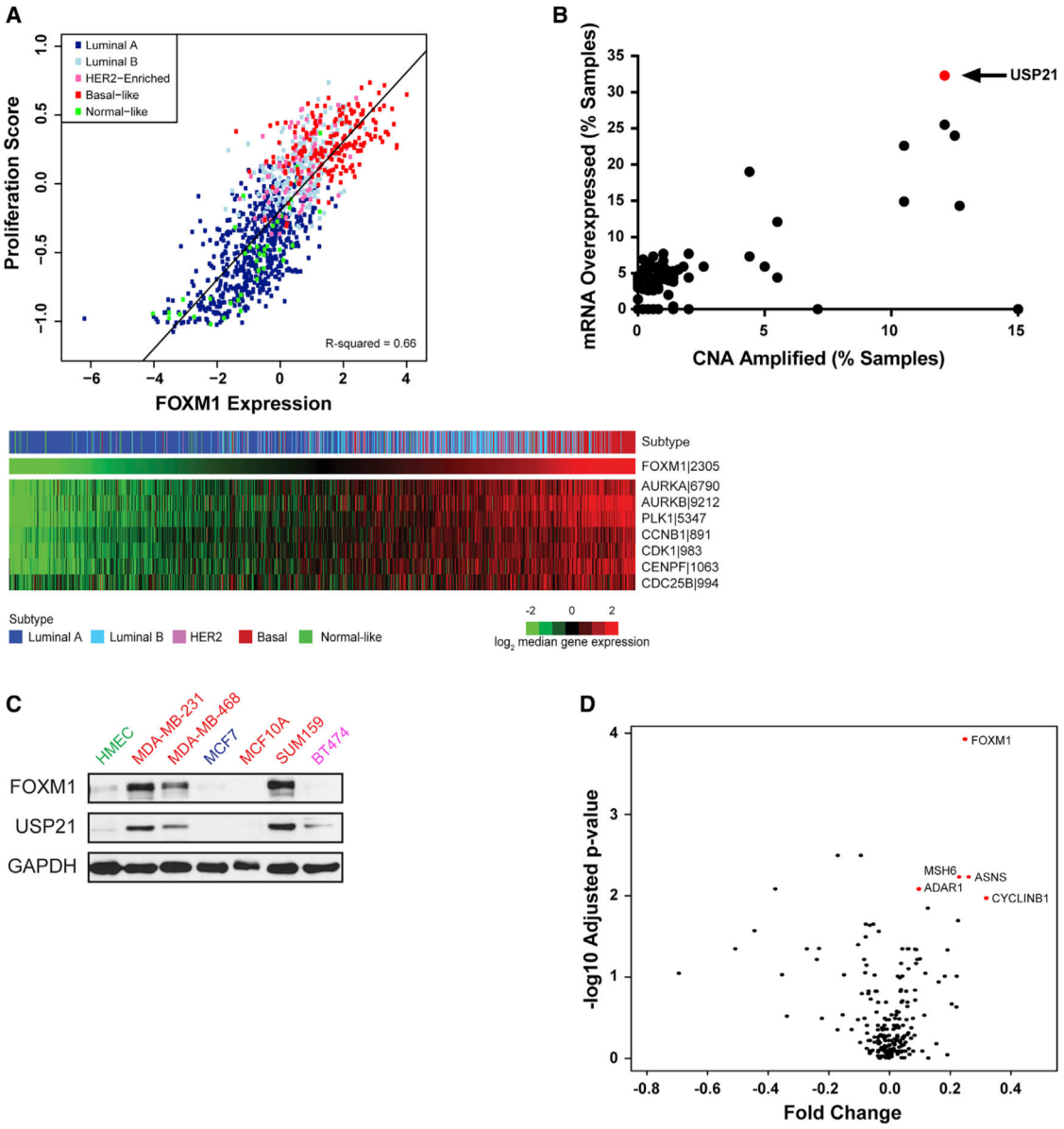

Figure 4. Amplification of FOXM1 and USP21 Is Linked to Proliferation in BLBC

(A) Top: log2 median FOXM1 expression in TCGA breast cancers compared with proliferation score and subtype. Bottom: log2 median FOXM1 expression and 7 FOXM1 target genes ordered by FOXM1 expression. PAM50 breast cancer subtypes: basal like, red; HER2 enriched, hot pink; luminal A, dark blue; luminal B, light blue; normal like, green.

(B) Analysis comparing mRNA overexpression (Z score threshold ± 2) and CNA amplification of 92 DUBs in 482 tumor samples from the TCGA breast invasive carcinoma dataset.

(C) FOXM1 and USP21 abundance assessed by IB in a panel of breast cancer cell lines. Breast cancer subtype denoted by color (normal, green; luminal, blue; HER2, pink; BLBC, red).

(D) Volcano plot showing protein expression levels in USP21-amplified patient tumors based on RPPA data from the TCGA breast cancer dataset.

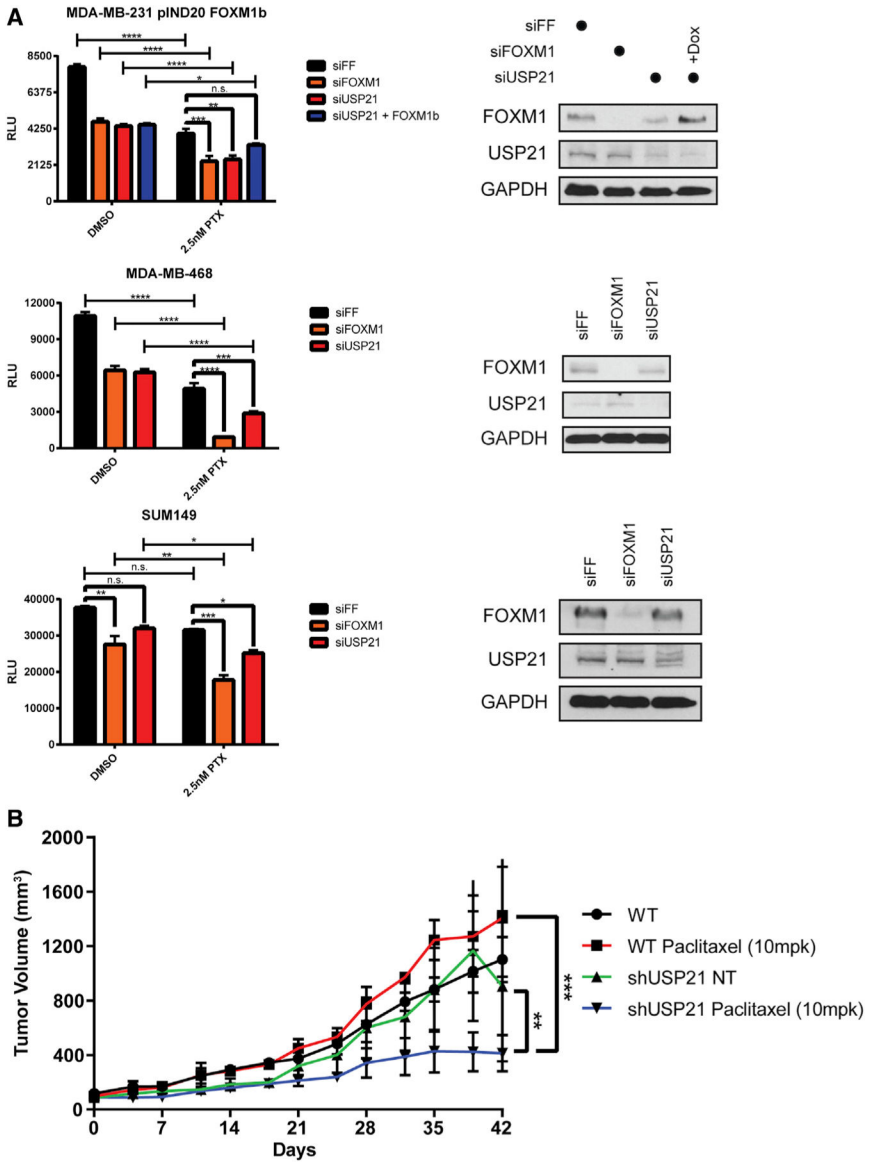

Figure 5. USP21 Knockdown Sensitizes BLBC Cells to Paclitaxel

(A) Relative viability of MDA-MB-231 cells (pINDUCER20 FOXM1b transduced) (top), MDA-MB-468 cells (middle), and SUM149 cells (bottom) treated with the indicated siRNA and exposed to the indicated concentration of paclitaxel (and 10 ng/mL of doxycycline [Dox] in siUSP21 + Dox) for 72 h. Each condition represents mean of triplicates. Error bars represent SEM. *p ≤ 0.05, **p ≤ 0.01, ***p ≤ 0.001, and ****p ≤ 0.0001 based on two-way ANOVA with post hoc pairwise analysis. IB confirming expression of FOXM1 and USP21 is shown to the right for each corresponding experiment.

(B) Quantification of mean tumor volume of SUM149 mouse xenograft for the indicated conditions. For each condition, n = 3. Error bars represent SEM. **p ≤ 0.01 and ***p ≤ 0.001 based on paired t test of respective measurements.

KEY RESOURCES TABLE

REAGENT or RESOURCE	SOURCE	IDENTIFIER
Antibodies		
Aurora A	CST	Cat# 13092; RRID: AB_2061342
CCP110	Bethyl	Cat# A301–343A; RRID: AB_937760
CDK1	Bethyl	Cat# A303–663A; RRID: AB_11205291
Cyclin B1	Abcam	Cat# ab32053; RRID: AB_731779
Cyclin E1	CST	Cat# 4129; RRID: AB_2071200
FLAG M2	Sigma-Aldrich	Cat# F1804; RRID: AB_262044
FOXM1	Santa Cruz	Cat# sc-502; RRID: AB_631523
GAPDH	Santa Cruz	Cat# sc-25778; RRID: AB_10167668
Goat Anti-Mouse IgG (H+L) HRP	Jackson ImmunoResearch	Cat# 115-035-003; RRID: AB_10015289
Goat Anti-Mouse IgG (L) HRP	Jackson ImmunoResearch	Cat# 115-035-174; RRID: AB_2338512
Goat Anti-Rabbit IgG (H+L) Alexa Fluor 488	Thermo Fisher	Cat# A-11034; RRID: AB_2576217
Goat Anti-Rabbit IgG (H+L) HRP	Jackson ImmunoResearch	Cat# 111-035-003; RRID: AB_2313567
GST	Gene Tex	Cat# GTX114099; RRID: AB_1949436
HA	Covance	Cat# MMS-101P; RRID: AB_2314672
Mouse Anti-Rabbit IgG (L) HRP	Jackson ImmunoResearch	Cat# 211-032-171; RRID: AB_2339149
Myc	Santa Cruz	Cat# sc-40; RRID: AB_627268
Normal Mouse IgG	Santa Cruz	Cat# sc-2025; RRID: AB_737182
Phospho-Histone H3 S10	CST	Cat# 3377; RRID: AB_1549592
Tubulin	Santa Cruz	Cat# sc-32293; RRID: AB_628412
USP21	This Paper	N/A
Bacterial and Virus Strains		
Escherichia coli BL21(DE3) Chemically Competent Cells	Thermo Fisher	Cat# C600003
Chemicals, Peptides, and Recombinant Proteins		
Aphidicolin	MilliporeSigma	Cat# A0781
Clarity ECL Western Blotting Substrate	Bio-Rad	Cat# 1705060
Cycloheximide	MilliporeSigma	Cat# 01810
EZView Red Anti-HA Affinity Gel	MilliporeSigma	Cat# E6779
Glutathione Agarose Resin	GoldBio	Cat# G-250–5
HisPur Ni-NTA Resin	Thermo Fisher	Cat# 88221
Lipofectamine 2000	Thermo Fisher	Cat# 11668027
Lipofectamine RNAiMAX	Thermo Fisher	Cat# 13778150
Matrigel Basement Membrane Mix	BD Biosciences	Cat# 356234
MG132	Selleck Chemicals	Cat# S2619
Nocodazole	MilliporeSigma	Cat# M1404
Pierce ECL Western Blotting Substrate	Thermo Fisher	Cat# 32106
PR-619	Selleck Chemicals	Cat# S7130
Propidium Iodide	MilliporeSigma	Cat# P4864
RNase A	MilliporeSigma	Cat# R6513

REAGENT or RESOURCE	SOURCE	IDENTIFIER
SsoAdvanced SYBR Green	Bio-Rad	Cat# 1725271
SureBeads Protein A and G	Bio-Rad	Cat# 1614833
TransIT-293 Reagent	Mirus Bio	Cat# MIR 2700
Zeba Desalting Columns	Thermo Fisher	Cat# 89889
Peptide (USP21 Antibody): PASGPNPMLRPLPPR	This Paper	N/A
GST-USP21	This Paper	N/A
6HIS-FOXM1b	This Paper	N/A
Critical Commercial Assays		
Luciferase Assay System	Promega	Cat# E1500
Pierce BCA Protein Assay Kit	Thermo Fisher	Cat# 23225
PrestoBlue Cell Viability Reagent	Thermo Fisher	Cat# A13261
QuickChange Lightning Site-Directed Mutagenesis Kit	Agilent	Cat# 210518
RNeasy Mini Kit	QIAGEN	Cat# 74104
SuperScript III First-Strand Synthesis System	Thermo Fisher	Cat# 18080051
Experimental Models: Cell Lines		
293T	ATCC	Cat# CRL-3216; RRID: CVCL_0063
BT474	ATCC	Cat# HTB-20; RRID: CVCL_0179
HeLa	ATCC	Cat# CCL-2; RRID: CVCL_0030
HMEC	ATCC	Cat# PCS-600–010
MCF10A	ATCC	Cat# CRL-10317; RRID: CVL_0598
MCF7	ATCC	Cat# HTB-22; RRID: CVCL_0031
MDA-MB-231	ATCC	Cat# HTB-26; RRID: CVCL_0062
MDA-MB-468	ATCC	Cat# HTB-132; RRID: CVCL_0419
SUM149	BioIVT (Astrand)	RRID: CVCL_3422
SUM159	BioIVT (Astrand)	RRID: CVCL_5423
Experimental Models: Organisms/Strains		
Mouse: BALB/c female nude (nu/nu)	UNC-CH MP1U	N/A
Oligonucleotides		
See Table S2 for qPCR, SDM, shRNA and siRNA primer lists		N/A
Recombinant DNA		
6HIS-FLAG-Ubiquitin	Gift from Philippe Soubeyran	N/A
6x-DBE FOXM1 Luc Reporter	Gift from Michael Whitfield (Dartmouth Univ)	N/A
MSCV-FLAG-HA-USP21	Sowa et al., 2009	Addgene Plasmid #22574
MSCV-FLAG-HA-USP21 C221A	This Paper	N/A
MSCV-FLAG-HA-USP21 siResist	This Paper	N/A
pDEST-FLAG-FOXM1b	This Paper	N/A
pDEST-HA-FOXM1b	This Paper	N/A
pDEST-Myc-FOXM1b 1–160	This Paper	N/A
pDEST-Myc-FOXM1b 161–320	This Paper	N/A
pDEST-Myc-FOXM1b 235–480	This Paper	N/A
pDEST-Myc-FOXM1b 321–480	This Paper	N/A

REAGENT or RESOURCE	SOURCE	IDENTIFIER
pDEST-Myc-FOXM1b 350–480	This Paper	N/A
pDEST-Myc-FOXM1b 400–530	This Paper	N/A
pDEST-Myc-FOXM1b 450–580	This Paper	N/A
pDEST-Myc-FOXM1b 480–625	This Paper	N/A
pDEST-Myc-FOXM1b 481–640	This Paper	N/A
pDEST-Myc-USP21	This Paper	N/A
pDEST15-GST-USP21	This Paper	N/A
pDONR223-FOXM1b	This Paper	N/A
pDONR223-USP21	This Paper	N/A
pET-28b-FOXM1b	This Paper	N/A
pINDUCER20	Meerbrey et al., 2011	Addgene Plasmid #44012
pINDUCER20-FOXM1b	This Paper	N/A
pINDUCER20-USP21	This Paper	N/A
pLKO.1 shNonT	MilliporeSigma	Cat# SHC016
pLKO.1 shUSP21	This Paper	N/A
Software and Algorithms		
FlowJo X	FlowJo LLC	https://www.flowjo.com
ImageJ		https://imagej.nih.gov
Prism 6	GraphPad	https://www.graphpad.com
R		https://www.r-project.org
Other		
CyAn ADP Analyzer	Beckman Coulter	N/A
IncuCYTE Zoom	Essen Bioscience	N/A
QuantStudio 7 Flex Real-Time PCR System	Thermo Fisher	N/A